Reconstructing non-Markovian open quantum evolution from multiple time measurements

Chu Guo *

Henan Key Laboratory of Quantum Information and Cryptography, Zhengzhou, Henan 450000, China
and Key Laboratory of Low-Dimensional Quantum Structures and Quantum Control of Ministry of Education, Department of Physics
and Synergetic Innovation Center for Quantum Effects and Applications, Hunan Normal University, Changsha 410081, China

(Received 3 May 2022; accepted 5 August 2022; published 15 August 2022)

For a quantum system undergoing non-Markovian open quantum dynamics, we demonstrate a tomography algorithm based on multitime measurements of the system, which reconstructs a minimal environment coupled to the system, such that the system plus environment undergoes unitary evolution and that the reduced dynamics of the system is identical to the observed dynamics of it. The reconstructed open quantum evolution model can be used to predict any future dynamics of the system when it is further assumed to be time-independent. We define the memory size and memory complexity for the non-Markovian open quantum dynamics which characterize the complexity of the reconstruction algorithm.

DOI: 10.1103/PhysRevA.106.022411

I. INTRODUCTION

A quantum system is almost inevitably affected by some environment, in which case the dynamics has to be described in the context of an open quantum system [1]. A powerful tool to study an open quantum system is the quantum map (or quantum channel), which is a linear and completely positive (CP) mapping from a quantum state at a time t_0 to another quantum state at a later time t_1, denoted as $\mathcal{E}_{1:0}$ [2,3]. Given a microscopic description for the unitary evolution of the quantum system plus an environment [4], a reduced quantum map acting only on the system can be computed by tracing out the environment. However, the details of the environment affecting the quantum system may not be clear *a priori*, which is usually the case for noisy near-term quantum devices [5–7]. Nevertheless, given experimental access to prepare an arbitrary initial state of the system and measure the system later, the unknown quantum map can also be systematically reconstructed using quantum process tomography (QPT) [8,9].

However, the quantum map cannot fully characterize the non-Markovian open quantum dynamics; for example, if we consider the quantum map between t_0 and another time $t_2 > t_1$ in the non-Markovian case, the equality $\mathcal{E}_{2:0} = \mathcal{E}_{2:1}\mathcal{E}_{1:0}$ does not hold in general [10,11]. In other words, to characterize the quantum dynamics between t_0 and any time t, one may have to perform a QPT separately for each t, which is of course undesirable. In such situations, a natural question to ask is: given preparation and measurement accesses to the underlying quantum system, can we build a model which fully characterizes the non-Markovian open quantum dynamics of it (for example, to predict the quantum state at arbitrary times)?

The first step to answer this question is to give an informationally complete description of the non-Markovian open quantum dynamics. For this purpose, we look at the classical stochastic process as a reference, which describes a sequence of random variables $X_{k:0} = X_0 X_1 \cdots X_k$ (the starting time in literatures is usually chosen as $-\infty$ since one is often concerned with the stationary stochastic process, but here we choose it to be 0 for correspondence with the quantum case) [12]. A Markovian stochastic process can be fully characterized by the transition matrix, $P(X_k|x_{k-1})$, with x_{k-1} a specific state at time $k-1$. In comparison, a non-Markovian stochastic process should be characterized by the conditional probabilities on the all the possible histories: $P(X_k|x_{k-1:0})$, where $x_{k-1:0} = \{x_0, \ldots, x_{k-1}\}$ denotes a specific history. Given these facts, the connection between a quantum process and a classical stochastic process can be easily drawn as follows. The quantum state ρ_k at time step k is similar to the random variable X_k. The quantum map $\mathcal{E}_{k:k-1}$ is similar to the transition matrix since it is the current state ρ_k conditioned on the last preparation of the input quantum state, denoted as $\mathcal{P}_{k-1}$, which can thus be written as $\mathcal{E}_{k:k-1} = \rho_k(\mathcal{P}_{k-1})$. Given these correspondences, it is clear that to fully characterize the non-Markovian quantum dynamics, a mapping $\rho_k(\Lambda_{k-1:0})$ corresponding to $P(X_k|x_{k-1:0})$ is still needed, which is the current state ρ_k conditioned on a sequence of history quantum operations $\Lambda_{k-1:0} = \{\Lambda_0, \ldots, \Lambda_{k-1}\}$ at k different times $\{t_0, \ldots, t_{k-1}\}$. Since each quantum operation Λ_j can be implemented by a measurement $\mathcal{M}_j$ followed by a preparation $\mathcal{P}_j$ [13], this mapping can also be denoted as $\rho_k(\mathcal{P}_{k-1:0}, \mathcal{M}_{k-1:0})$. The last expression actually closely resembles a special instance of classical stochastic process, the *transducer with memory*, which models a system that emits a random variable Y_j (which corresponds to $\mathcal{M}_j$) given an input random variable X_{j-1} (which corresponds to $\mathcal{P}_{j-1}$) at each time j (in the meantime some "hidden memory state" changes which corresponds to the collapse of the quantum state upon measurement) and is fully characterized by the conditional probability $P(Y_k|X_{k-1:0}, Y_{k-1:0})$ [12]. The mapping $\rho_k(\Lambda_{k-1:0})$ is exactly a k-step *process tensor* as discovered recently, which is a linear and CP mapping from a sequence of quantum operations $\Lambda_{k-1:0}$ to the output quantum state ρ_k; moreover, the process tensor represents the most

*guochu604b@gmail.com

generic quantum measurements one could possibly perform on a quantum system [14,15].

The conditional probability $P(X_k|x_{k-1:0})$ and the process tensor $\rho_k(\Lambda_{k-1:0})$ fully characterize a classical stochastic process and a quantum process, respectively. However, these descriptions alone are not efficient since the possible histories, namely, $x_{k-1:0}$ and $\Lambda_{k-1:0}$, grow exponentially with k. In the classical case, this problem is solved by constructing a *predictive model* from the observed data $P(X_k|x_{k-1:0})$ (ideally using only a finite k). The ϵ-machine is an outstanding predictive model [16], which also belongs to the broader class of hidden Markov models. Briefly, instead of storing all the $P(X_k|x_{k-1:0})$ for any k, the ϵ-machine divides the histories $x_{k-1:0}$ into disjoint classes, denoted as $\epsilon(x_{k-1:0})$. Each class is referred to as a causal state and represents all the histories that give the same current state, that is, $P(X_k|x_{k-1:0}) = P(X_k|x'_{k-1:0})$ for all $x'_{k-1:0} \in \epsilon(x_{k-1:0})$. In the quantum case, a natural predictive model exists, which is referred to as the open quantum evolution (OQE) model and is defined as follows: the system interacts with an (unknown) environment, such that the system plus environment undergoes unitary evolution and that the observed non-Markovian quantum dynamics is the reduced dynamics of the system after tracing out the environment. However, it is currently unknown how to reconstruct an OQE model based on experimentally measurable quantities (the process tensor), such that the non-Markovian quantum dynamics of the system is fully characterized.

This gap is filled in this work. We first present an efficient algorithm for process tensor tomography, the complexity of which grows exponentially with the memory complexity (which will be defined later), but only linearly with k. On top of that, we show that the hidden OQE model can be further reconstructed with little overhead. Briefly, this work gives a systematic and efficient way to reconstruct the quantum predictive model (OQE), which encodes all the information about the non-Markovian quantum dynamics. The algorithm is demonstrated with numerical examples.

II. THE PURIFIED PROCESS TENSOR

Before presenting the main results of this work, we will first briefly review the process tensor framework [15] and define the purified form of the process tensor (PPT), which will be useful for the later proofs.

The quantum map has been a conventional and powerful tool to study open quantum dynamics, which can be obtained from all the possible two-time measurements, namely, preparing an arbitrary initial state and then performing quantum state tomography (QST) at a later time. However, in the non-Markovian case the quantum map alone cannot accurately predict the future dynamics, which is essentially because that the non-Markovian quantum dynamics cannot be fully characterized using two-time measurements only. Nevertheless, the two-time measurement can be naturally generalized to multiple times; namely, one performs k quantum operations at k different times from t_0 to t_{k-1}, denoted as $\Lambda_{k-1:0}$, and then performs a QST at time t_k to obtain the final quantum state ρ_k of the system. Similar to quantum map, the mapping from $\Lambda_{k-1:0}$, denoted as $\rho_k(\Lambda_{k-1:0})$, to ρ_k is defined as the k-step process tensor. Since arbitrary non-Markovian quantum dynamics can be understood as the reduced dynamics from the coupling to some environment, the process tensor could also be more explicitly defined based on the hidden OQE model as [15]

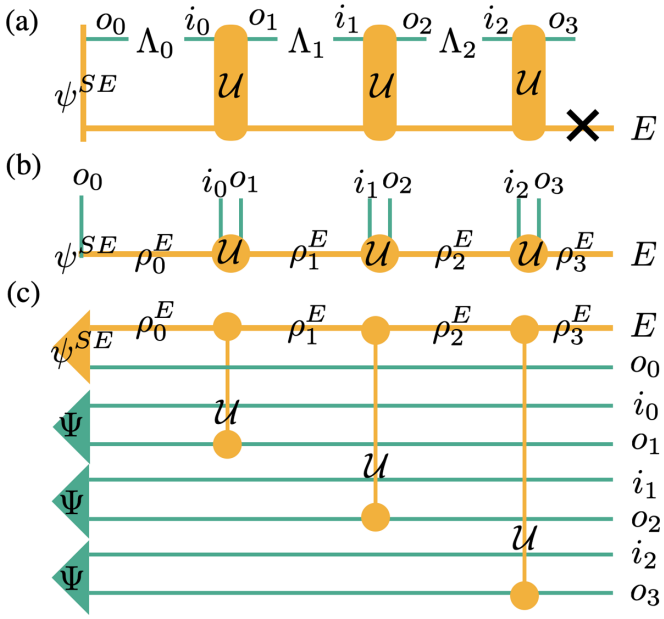

FIG. 1. (a) Demonstration of a three-step process tensor under a hidden OQE model, for which $\mathcal{U}$ is the unitary evolutionary operator for the system plus the environment, and $|\psi^{SE}\rangle$ is the system-environment initial state. i_j and o_j are the jth input and output indices, respectively. (b) The matrix product state representation of the purified process tensor, for which the environment is not traced out in the end. (c) The quantum circuit implementation of the purified process tensor as a many-body pure state, where $|\Psi\rangle$ is the maximally entangled state. The process tensor is obtained by tracing out the environment index. ρ_j^E in (b) and (c) denotes the jth effective environment state in Eq. (15).

$$\rho_k(\Lambda_{k-1:0}) = \mathrm{tr}_E\left(\mathcal{U}_{k:k-1}\Lambda_{k-1}\cdots\mathcal{U}_{1:0}\Lambda_0\rho_0^{SE}\right), \tag{1}$$

where ρ_0^{SE} is the system-environment (SE) initial state and $\mathcal{U}_{j:j-1}$ is the SE unitary evolutionary operator from time step $j-1$ to j, namely, $\mathcal{U}_{j:j-1}\rho^{SE} = U_{j:j-1}\rho^{SE}U_{j:j-1}^\dagger$ with $U_{j:j-1}$ a unitary matrix. We further assume ρ_0^{SE} to be a pure state: $\rho_0^{SE} = |\psi^{SE}\rangle\langle\psi^{SE}|$. This assumption does not lose any generality since if ρ_0^{SE} is a mixed state; one can purify it by adding external degrees of freedom and enlarging $\mathcal{U}$ accordingly. The process tensor is demonstrated in Fig. 1(a). Based on Eq. (1), it has been shown that the process tensor is a linear and CP mapping [15], which immediately inspires a tomography algorithm for the process tensor similar to the standard QPT: one prepares $\Lambda_{k-1:0}$ with each Λ_j selected from an informationally complete set and then performs QST on the output quantum state [17]. For system size d, the total number of configurations grows as d^{4k+2} (since each Λ_j lives in a linear space of size $d^2 \times d^2$ and ρ_k lives in a space of size $d \times d$), which will soon become unfeasible for relatively small k, and as a result the largest experiment for process tensor tomography to date uses $k \leqslant 3$ [18–20]. In the following we will also denote the k-step process tensor as $\Upsilon_{k:0}$ for brevity.

The PPT can be defined similar to Eq. (1), but without tracing out the environment index in the end, which is shown in Fig. 1(b). We can see that the PPT is similar to a pure quantum state and can be naturally written as a matrix product state (MPS):

$$|\Upsilon_{k:0}\rangle = \sum_{o_{k:0},i_{k-1:0},\alpha_{k-1:0}} B^{o_0}_{\alpha_0} B^{i_0,o_1}_{\alpha_0,\alpha_1} \cdots B^{i_{k-1},o_k}_{\alpha_{k-1},\alpha_k} \times |\alpha_k\rangle |o_{k:0}, i_{k-1:0}\rangle, \tag{2}$$

where $o_{k:0} = \{o_0, \ldots, o_k\}$ and similarly for $i_{k-1:0}$ and $\alpha_{k-1:0}$. i_j, o_j are the "physical indices" which correspond to particular choices of basis for $\mathcal{P}_j$ and $\mathcal{M}_j$, respectively, andα_j is the "auxiliary index" corresponding to a choice of basis for the environment after the jth step. The site tensor $B^{o_0}_{\alpha_0} = \langle o_0, \alpha_0 | \psi^{SE} \rangle$ is a redefinition of the SE initial state, while $B^{i_{j-1},i_j}_{\alpha_{j-1},\alpha_j}$ with $j \geqslant 1$ is simply a redefinition of the unitary matrix $U_{j:j-1}$. It is often convenient to view each site tensor of the PPT as a list of matrices B^{i_{j-1},o_j}, which are labeled by the physical indices i_{j-1}, o_j and act on the auxiliary index (environment) only (B^{o_0} is a list of vectors). The *bond dimension* of an MPS is defined as the size of each auxiliary index α_j, which characterizes the size of each site tensor. The MPS representation in Eq. (2) is naturally right-canonical since each site tensor satisfies the right-canonical condition [21,22]

$$\sum_{i_{j-1},o_j,\alpha_j} B^{i_{j-1},o_j}_{\alpha_{j-1},\alpha_j} \left(B^{i_{j-1},o_j}_{\alpha'_{j-1},\alpha_j}\right)^* = \delta_{\alpha_{j-1},\alpha'_{j-1}}, \tag{3}$$

where we have used the unitary property of $U_{j:j-1}$. The process tensor can be obtained from the PPT by

$$\Upsilon_{k:0} = \mathrm{tr}_E(|\Upsilon_{k:0}\rangle\langle\Upsilon_{k:0}|) = \sum_{\alpha_k} \langle\alpha_k|\Upsilon_{k:0}\rangle\langle\Upsilon_{k:0}|\alpha_k\rangle. \tag{4}$$

It has been shown that the process tensor $\Upsilon_{k:0}$ for an environment with size D can be written as a matrix product density operator (MPDO) with bond dimension D [15]. Moreover, Eq. (4) shows that the process tensor is a very special MPDO; for example, given the PPT $|\Upsilon_{k:0}\rangle$ with bond dimension D, one can obtain the process tensor $\Upsilon_{k:0}$ as an MPDO with bond dimension D by Eq. (4). However, an MPDO with bond dimension D in general can not be purified into the form of PPT with the same bond dimension [23–26]. This speciality of the process tensor is central to the efficient tomography algorithm we propose for it, which will be shown later.

Interestingly, the PPT can also be implemented using the quantum circuit shown in Fig. 1(c) (we note that in the original definition of the quantum circuit SWAP gates have been used since physically only the quantum system corresponding to the index o_0 may directly interact with the environment [15]), which converts the PPT defined at multiple times into a multiqubit many-body quantum state. This can be seen by verifying the outcome of each gate operation simultaneously acting on o_j and the environment index

$$\mathcal{U}|\Psi\rangle = \mathcal{U}|\alpha\rangle \frac{1}{\sqrt{d}} \sum_{j=1}^{d} |j\rangle_i |j\rangle_o = \frac{1}{\sqrt{d}} \sum_{j=1}^{d} |j\rangle_i (\mathcal{U}|\alpha\rangle|j\rangle_o) = \frac{1}{\sqrt{d}} \sum_{\beta,k,j} U^{j,k}_{\alpha,\beta} |\beta\rangle|k\rangle_o |j\rangle_i, \tag{5}$$

which is indeed the jth site tensor of the PPT up to a factor $1/\sqrt{d}$ (here the state $|j\rangle$ with subscript i or o means that it corresponds to the input or output index). Thus the output of the quantum circuit in Fig. 1(c) without tracing out the environment is exactly the PPT up to a factor $(1/\sqrt{d})^k$. We also note that the quantum circuit in Fig. 1(c) is actually a way to prepare a given MPS on a quantum computer, known as the sequentially generated multiqubit state [27].

III. EFFICIENT OQE RECONSTRUCTION ALGORITHM

In the following we will first present an efficient algorithm to reconstruct the PPT based on experimental measurements, and then we show that the OQE can be reconstructed based on the obtained PPT with little or no additional effort. Since the process tensor is simply related to the PPT [see Eq. (4)], it can also be straightforwardly computed based on the obtained PPT.

The quantum circuit implementation of the (purified) process tensor as a many-body quantum state immediately motivates us to apply the techniques used for many-body QST for process tensor tomography. It has been shown that for pure or fairly pure (a mixed quantum state which can be written as the sum of a few pure states [28]) quantum states there exist efficient tomography algorithms with guaranteed convergence, which scales only linearly with the system size [29–31]. These algorithms, however, do not work for a generic MPDO since the latter could easily represent highly mixed quantum states even with a very small bond dimension (1, for example). Nevertheless, as we have pointed out, the process tensor is a very special MPDO, and we will show that it allows efficient tomography if one assumes that the size of the unknown environment is bounded by some integer D (also see Refs. [32,33] for a heuristic tensor network-based machine learning algorithm to directly reconstruct the process tensor as an matrix product operator).

Instead of directly reconstructing the process tensor, we will reconstruct the PPT instead, which can be done with tomography of the output quantum state of the quantum circuit in Fig. 1(c). At first sight this seems impossible due to the existence of the environment index in the circuit, which is assumed to be not directly accessible. However, as will be shown, we could freely select a particular environment basis in the end since it does not affect the process tensor (the PPT itself is not directly experimentally measurable and could be dependent on the environment basis). Following Ref. [29], and assuming that the unknown environment has a size bounded by D, one can apply a disentangling quantum circuit onto the (unknown) PPT and get

$$O_f \cdots O_1 O_0 |\Upsilon_{k:0}\rangle = |0\rangle_{f:0} \otimes \sum_s \lambda_s |a_s\rangle |b_s\rangle_E, \tag{6}$$

with $\kappa = \lceil \log_{d^2}(D) \rceil + 1$, $f = k - \kappa + 1$, and k the total number of time steps (sites). $|0\rangle_{f:0}$ means the product state of $|0\rangle$ for site 0 and $|00\rangle$ for sites 1 to f. O_j is the jth disentangling gate acting on κ sites from j to $j + \kappa - 1$, defined as [29]

$$O_j = \sum_{r=0}^{d^2-1} \sum_{r'=0}^{d^{2(\kappa-1)}-1} |r\rangle_1 \otimes |r'\rangle_{\kappa:2} \langle \phi_{rd^{2(\kappa-1)}+r'+1}|_{\kappa:1}, \tag{7}$$

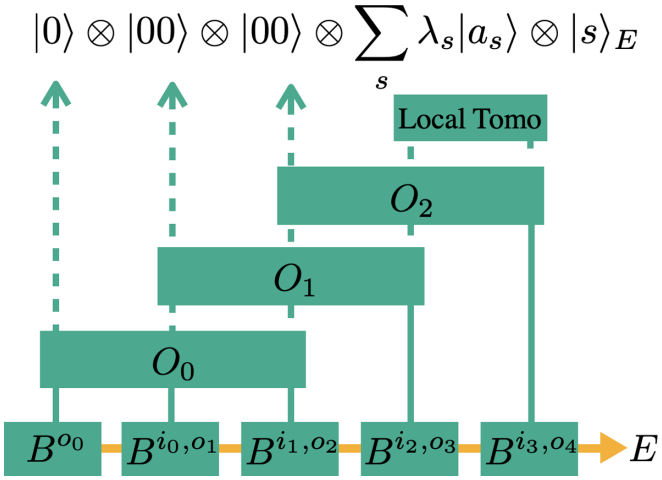

FIG. 2. Demonstration of the efficient purified process tensor tomography algorithm for a four-step purified process tensor, where we have assumed that the environment size $D \leqslant d^4$. The unitary gate O_j is the jth disentangling operator in Eq. (7). $|a_s\rangle$ is the sth eigenstate of the reduced density matrix on the last two sites, and λ_s is the square root of the corresponding eigenvalue.

where $|r\rangle_1$ denotes the computational basis for site j and $|r'\rangle_{\kappa:2}$ the computational basis from sites $j+1$ to $j+\kappa-1$, and $|\phi_l\rangle$ denotes the lth eigenstate of the reduced density matrix (reduced process tensor) $\Upsilon_{j+\kappa-1:j}$ obtained by local QST of sites j to $j+\kappa-1$ after the previous gate operations O_0 to O_{j-1} have been applied (the $|\phi_l\rangle$s are sorted according to the eigenvalues from large to small). $|a_s\rangle$ and λ_s^2 are the eigenstates and eigenvalues of $\Upsilon_{k:k-\kappa+1}$, which can be obtained by local QST of the last $k-\kappa$ sites after all the gate operations have been applied. $|b_s\rangle_E$ is a set of unknown orthogonal states for the environment. Since we can arbitrarily change the environment basis without any observable effects (the environment will be traced out when computing the process tensor or any observables), we can simply choose $|b_s\rangle_E$ as the computational basis, denoted as $|s\rangle_E$. Therefore the quantum state on the right-hand side of Eq. (6) is fixed, and we can easily obtain the PPT as an MPS on a classical computer by applying the inverse of the disentangling quantum circuit onto this state, namely,

$$|\Upsilon_{k:0}\rangle = O_0^\dagger O_1^\dagger \cdots O_f^\dagger |0\rangle_{f:0} \otimes \sum_s \lambda_s |a_s\rangle |s\rangle_E. \tag{8}$$

This purified process tensor tomography algorithm requires $k-\kappa+2$ local QSTs on κ sites, as demonstrated in Fig. 2; therefore the complexity of this algorithm is $O((k-\kappa+2)\times d^{2\kappa})$ (the complexity of the intermediate gate operations is ignored).

From Eq. (2), the hidden OQE model can be straightforwardly obtained once we have obtained the MPS for a k-step PPT. In principle one only needs to prepare the obtained MPS into the right-canonical form, and then the site tensors will naturally reveal the hidden OQE model; that is, the first site tensor is the SE initial state and the rest are the SE unitary evolutionary operators. However, in general a site tensor satisfying the right-canonical condition does not guarantee that it is a unitary matrix as in Eq. (2) up to the factor $1/\sqrt{d}$ [the unitary property of the site tensor implies the right canonical condition in Eq. (3) but the reverse is not true]; the latter is only guaranteed by the physics: the obtained MPS has to result from some hidden OQE model since it is the most general description of an open quantum dynamics [1]. In practice, if one loses some precision during the PPT tomography, this property will not exactly hold. Nevertheless, we could enforce a unitary SE evolutionary operator for each time step by an additional maximally likelihood estimation (MLE). Concretely, one can first find the unitary matrix $\tilde{U}_{j:j-1}$ closest to each $B^{i_{j-1},o_j}_{\alpha_{j-1},\alpha_j}$ obtained from the PPT tomography (this step is not necessary but could be helpful to obtain a good starting point for the next step), then one can further optimize each $\tilde{U}_{j:j-1}$ by minimizing the loss function

$$\text{loss}(\tilde{U}_{1:0}, \ldots, \tilde{U}_{k:k-1}) = ||\tilde{\Upsilon}_{k:0}\rangle - |\Upsilon_{k:0}\rangle|^2, \tag{9}$$

where $|\cdot|^2$ means the square of the Euclidean norm. $|\Upsilon_{k:0}\rangle$ means the PPT obtained from tomography and $|\tilde{\Upsilon}_{k:0}\rangle$ is the predicted PPT obtained by substituting all $\tilde{U}_{j:j-1}$ into Eq. (2). We note that the MLE procedure is purely done on a classical computer.

In certain cases one may assume that the influence of the environment on the system does not change with time; that is, there exists an OQE model with a constant evolutionary operator for any time step. Under this assumption, one can again first obtain a $\tilde{U}$ that is closest to some $B^{i_{j-1},o_j}_{\alpha_{j-1},\alpha_j}$ with a large j, and then obtain the optimal OQE model by minimizing the loss function

$$\text{loss}_c(|\tilde{\psi}^{SE}\rangle, \tilde{U}, \tilde{U}^E) = |\tilde{U}^E|\tilde{\Upsilon}_{k:0}\rangle - |\Upsilon_{k:0}\rangle|^2, \tag{10}$$

where $|\tilde{\psi}^{SE}\rangle$ is a parameterized pure SE initial state [corresponding to $\tilde{U}_{1:0}$ in Eq. (9)], and $|\tilde{\Upsilon}_{k:0}\rangle$ is obtained by substituting $|\tilde{\psi}^{SE}\rangle$ and $\tilde{U}$ into Eq. (2). $\tilde{U}^E$ is a parameterized unitary matrix acting on the environment only and is added to compensate the specific choice of basis for the final environment in Eq. (8). $\tilde{U}^E$ is not needed in Eq. (9) since it can be absorbed into $\tilde{U}_{k:k-1}$.

A toy model

To demonstrate the reconstruction algorithm for the PPT and the hidden OQE, we consider a simple toy model in which a quantum system with Hilbert space size d is coupled to an environment with size D. The SE unitary evolutionary operator is assumed to be

$$U = e^{-\mathrm{i}(I^{SE} + \eta H^{SE})}, \tag{11}$$

where I^{SE} is the identity matrix and H^{SE} is a random Hermitian matrix generated by the normal distribution. We consider a separable SE initial state for briefness:

$$|\psi^{SE}\rangle = |\psi^S\rangle \otimes |\psi^E\rangle, \tag{12}$$

where $|\psi^S\rangle$ and $|\psi^E\rangle$ are both randomly generated.

Concretely, we consider $d=2$, $D=5$, and $\eta=0.1$ in our numerical simulation. Our reconstruction algorithm runs in two stages. In the first stage we use the efficient PPT tomography algorithm to reconstruct the k-step PPT based on the quantum circuit implementation of the PPT in Fig. 1(c), and in the second stage we further minimize the loss function in

Eq. (10) based on the obtained PPT to reconstruct the OQE model. It turns out that in the second stage $k = 3$ is enough for us to accurately reconstruct the OQE model, thus we focus on reconstructing the three-step PPT in the first stage (for which there are four sites in total). For $D = 5$ we have $\kappa = 3$; as a result in the first stage we need to do two three-site QSTs to get $\Upsilon_{0:2}$ and $\Upsilon_{1:3}$, plus a final two-site QST to get $\Upsilon_{2:3}$. The detailed procedures are shown as follows. First, we obtain $\Upsilon_{0:2}$ by a local QST of the 0th to 2nd sites; we diagonalize $\Upsilon_{0:2}$ and find that it only has five nonzero eigenvalues. With the information of the nontrivial eigenpairs of $\Upsilon_{0:2}$, we can construct a unitary operator O_0 according to Eq. (7), which acts on the 0th to 2nd sites. Then applying O_0 onto the PPT (the output of the quantum circuit in Fig. 1(c)], the 0th site will be disentangled with the rest of the sites and we do a local QST of the one to three sites in the next to get $\Upsilon_{1:3}$. With $\Upsilon_{1:3}$ we can compute O_1. By applying O_0 and O_1 onto the PPT, we disentangle the 0th and 1st sites from the rest and then we do a local QST on the 2nd to 3rd sites to obtain $\Upsilon_{2:3}$. Diagonalizing $\Upsilon_{2:3}$, we obtain λ_s and $|a_s\rangle$ as shown in Fig. 2. After that, the PPT $|\Upsilon_{0:3}\rangle$ is simply obtained as an MPS using Eq. (8). We note that in the PPT tomography algorithm the exact value of D does not have to be known beforehand; it can be determined by counting the number of nonzero eigenvalues of $\Upsilon_{0:2}$ and $\Upsilon_{1:3}$ instead.

The site tensors in the obtained $|\Upsilon_{0:3}\rangle$ are in general site-dependent even if they are generated by a time-independent unitary operator U. To enforce a site-independent $\tilde{U}$ we can further minimize the loss function in Eq. (10) in the second stage [the simplification caused by a separable SE initial state as in Eq. (12) is that we do not need to consider $|\tilde{\psi}^{SE}\rangle$ in Eq. (10), since we can simply choose $|\psi^E\rangle = |0^E\rangle$ for the environment and system index o_0 is separable from the rest of the PPT]. In particular, we gradually increase k from 1 to 3 in Eq. (10), and the optimal $\tilde{U}$ obtained for smaller k is used as the initial guess for minimization with larger k. Once we obtain the final optimal $\tilde{U}$, we know all the information of the non-Markovian quantum dynamics [we can compute any k-step process tensor by substituting $\tilde{U}$ into Eq. (1)]. As an example, we compute the four-site reduced process tensors $\tilde{\Upsilon}_{j+3:j}$ and compare them with the exact ones computed by substituting U directly into Eq. (1), which are shown in Fig. 3. We can see that $\tilde{U}$ obtained with $k = 3$ already predicts $\tilde{\Upsilon}_{j+3:j}$s, which are in excellent agreement with the exact ones.

We note that as a proof of principle demonstration of the reconstruction algorithm we have not considered the imperfections during the PPT tomography. The BFGS algorithm [34] is used to minimize the loss function in Eq. (10) in the second stage, and automatic differentiation is used to compute the gradient efficiently [35].

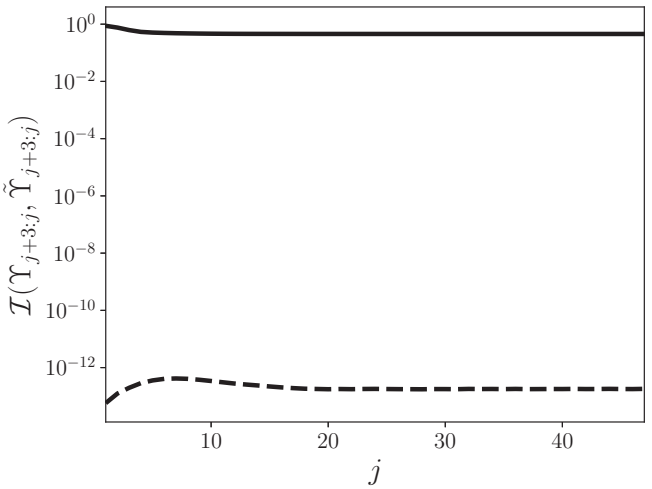

FIG. 3. Demonstration the tomography algorithm for reconstructing the hidden OQE model. The x axis is the time step j. The y axis is the infidelity $\mathcal{I} = 1 - \mathcal{F}$ ($\mathcal{F}(\rho, \sigma) = \mathrm{tr}^2(\sqrt{\sqrt{\rho}\sigma\sqrt{\rho}})$ is the quantum fidelity between two mixed states ρ and σ) between the reduced four-step process tensor $\Upsilon_{j+3:j}$ computed from the exact OQE model, and $\tilde{\Upsilon}_{j+3:j}$ predicted from the reconstructed OQE model. The black solid and dashed lines correspond to the results obtained by minimizing the loss function in Eq. (10) with $k = 2, 3$ respectively. The non-Markovian open quantum dynamics of the system is generated by a hidden OQE model with the unitary evolutionary operator U in Eq. (11) (with $d = 2$, $D = 5$, $\eta = 0.1$) and the SE initial state in Eq. (12).

IV. MEMORY SIZE AND MEMORY COMPLEXITY

In the following we will define the memory size and memory complexity for the non-Markovian open quantum dynamics, which are directly related to the complexity of reconstructing the PPT and the hidden OQE model. These two quantities also characterize the quantum process defined in Eq. (1) and are deeply related to the ϵ-machine.

Before introducing these two concepts, we first note that it has been shown that a classical stochastic process can also be simulated by the OQE model on a quantum computer, referred to as the q-simulator [36]. The q-simulator is a more efficient description of the classical stochastic process in that the environment size in a q-simulator could be exponentially smaller than the number of causal states in the ϵ-machine [37,38]. Moreover, the q-simulator has a one-to-one correspondence with an infinite MPS (iMPS) representation [39]. (In the classical case one is often interested in the stationary stochastic process, which would be described by an iMPS; a nonstationary stochastic process will correspond to a finite MPS instead as considered in this work.)

Drawing the similarity to the q-simulator and the iMPS representation for the classical stochastic process, we define the *memory size* of a quantum process after time step j, denoted as $\mathcal{D}_j$, as the Schmidt rank of the PPT in Eq. (2) at the jth bond (the leg corresponding to α_j):

$$\mathcal{D}_j = \dim(\alpha_j), \tag{13}$$

which is the size of the minimal environment at the jth bond which generates the next evolution. We also define the *memory complexity* of a quantum process after the jth time step as the quantum Rényi entropy of the PPT [39]

$$\mathcal{C}_j^\gamma = \frac{1}{1-\gamma} \log_2 \left[\mathrm{tr}\left(\Upsilon_{j:0}^\gamma\right)\right]. \tag{14}$$

The memory complexity defined in Eq. (14) can also be interpreted as the entanglement entropy of an *effective environment state* ρ_j^E after time step j, which carries all the history

information before (and include) the jth time step. Concretely, ρ_j^E is defined recursively as

$$\rho_j^E = \overleftarrow{T_j}\left(\rho_{j-1}^E\right) = \sum_{i_{j-1},o_j} (B^{i_{j-1},o_j})^\dagger \rho_{j-1}^E B^{i_{j-1},o_j}, \tag{15}$$

with $\rho_0^E = \mathrm{tr}_S(\rho_0^{SE})$ and T_j the jth transfer matrix of the PPT: $T_j = \sum_{i_{j-1},o_j} (B^{i_{j-1},o_j})^* \otimes B^{i_{j-1},o_j}$ [21,22]. $\overleftarrow{T_j}$ denotes the action of T_j on a state from the left. Matrix multiplication is understood for the environment indices in Eq. (15). Since the PPT in Eq. (2) is right-canonical, ρ_j^E is related to $\Upsilon_{k:j+1,E}$ (the reduced density matrix of $|\Upsilon_{k:0}\rangle$ corresponding to sites $j+1$ to k, plus the environment α_k) by an isometry (since each $B^{i_{j-1},o_j}_{\alpha_{j-1},\alpha_j}$ is an isometry from the Hilbert space $\mathcal{H}^E$ to $\mathcal{H}^E \otimes \mathcal{H}^S \otimes \mathcal{H}^S$). As a result ρ_j^E has the same entanglement entropy as $\Upsilon_{k:j+1,E}$ (thus also the same as $\Upsilon_{j:0}$ since $\Upsilon_{j:0}$ and $\Upsilon_{k:j+1,E}$ are the two bipartition reduced density matrices of the PPT $|\Upsilon_{k:0}\rangle$, which is a pure state). Therefore the memory complexity in Eq. (14) also measures the entropy of ρ_j^E. The importance of ρ_j^E can be further seen by considering a "local" measurement $\mathcal{M}_j$ (written as a matrix M_{o_j,o'_j})

$$\mathrm{tr}(\mathcal{M}_j \Upsilon_{j:0}) = \langle \Upsilon_{j:0}|\mathcal{M}_j|\Upsilon_{j:0}\rangle = \sum_{i_j,o_j,o'_j,\alpha_{j-1},\alpha'_{j-1},\alpha_j} \rho^E_{\alpha_{j-1},\alpha'_{j-1}} B^{i_{j-1},o_j}_{\alpha_{j-1},\alpha_j} M_{o_j,o'_j} \left(B^{i_{j-1},o'_j}_{\alpha'_{j-1},\alpha_j}\right)^*, \tag{16}$$

where "local" means that we perform preparations and measurements at all the previous time steps before j (instead of doing nothing) but average over them. From Eq. (16) we can see that to compute a local observable at time step j, all one needs from the past is ρ_{j-1}^E. In other words, ρ_{j-1}^E contains all the history information and fully determines the future quantum process and thus naturally corresponds to the distribution of the causal states in the ϵ-machine.

Now we can draw the connections between the classical stochastic process and the quantum process a step further. We have shown that the process tensor corresponds to the conditional probability on the histories, and that the OQE model corresponds to the ϵ-machine (more precisely the ϵ-transducer [40,41]). From the discussions above, we can further see that the minimal environment corresponds to the space spanned by all the memory states in the ϵ-machine and thus can be interpreted as the memory space. The memory size (the Schmidt rank of the PPT) is simply the size of the memory space. The effective environment state ρ_j^E corresponds to the (stationary) distribution of the classical causal states. The memory complexity corresponds to the classical memory complexity defined as the Rényi entropy of the (stationary) distribution of the causal states.

Additionally, we have the following theorem for the memory complexity of a quantum process defined in Eq. (1).

Theorem 1. Assuming that the non-Markovian open quantum dynamics is generated by a hidden OQE model which is time-independent with an environment size D, and that the dominate eigenstate of the transfer matrix T is nondegenerate, then $\mathcal{D}_\infty = D$, $\mathcal{C}_\infty^\gamma = \log_2(D)$ if ρ_0^{SE} is a pure state, and $\mathcal{D}_\infty = dD^2$, $\mathcal{C}_\infty^\gamma = \mathcal{C}_0^\gamma + \log_2(D)$ if ρ_0^{SE} is a mixed state with entanglement entropy $\mathcal{C}_0^\gamma$.

Proof. For pure ρ_0^{SE}, it suffices to show that $\rho_\infty^E = I^E/D$. For mixed ρ_0^{SE} with purification denoted as $|\rho_0^{SE}\rangle = \sum_s \lambda_s |x_s\rangle|y_s\rangle$, where $|x_s\rangle$ is an external orthogonal basis set, $|y_s\rangle$ an orthogonal basis set of the environment, and λ_s the Schmidt numbers, it suffices to show that $\rho_\infty^{E'} = \sum_s \lambda_s^2 |x_s\rangle\langle x_s| \otimes I^E/D$, where E' denotes the enlarged environment including the external basis. More details of the proof can be found in the Appendix. Interestingly, based on Theorem 1, one could use $\mathcal{C}_k^\gamma$ to detect the memory size $\mathcal{D}_k$ for a quantum process with large enough k, since the former is experimentally accessible [42,43].

From the above theorem we can see that the complexity of the PPT tomography (thus also the complexity of the reconstruction algorithm for the hidden OQE model) shown in Sec. III is bounded by $O(kd^2\mathcal{D}_\infty) = O(kd^2 2^{\mathcal{C}_\infty^\gamma})$ (for time-independent U we may be able to reconstruct the OQE model more efficiently with a very small k, as demonstrated in the toy model in Fig. 3). The growths of the memory complexity and the memory size with the time step are shown in Fig. 4, where the non-Markovian open quantum dynamics of the system is generated by a hidden OQE model with the unitary evolutionary operator in Eq. (11), but with the initial states to be randomly generated pure or mixed states which are not separable. We can see that both of them converge to their limiting values as predicted in Theorem 1.

V. DISCUSSION AND CONCLUSION

The foundations of the process tensor framework are laid in Ref. [15], which (1) provides a formal definition of the process tensor as a natural generalization of the quantum map and (2) shows that the process tensor can be written as a matrix product density operator. Our work provides some

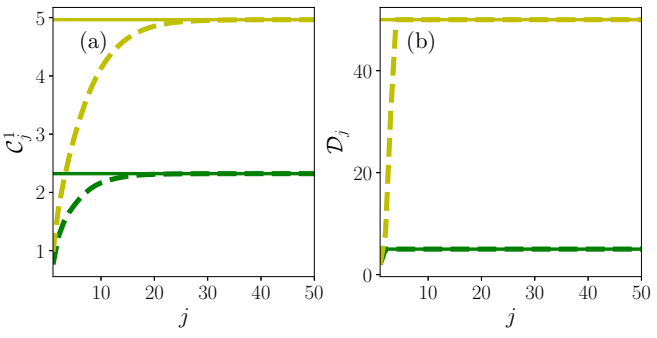

FIG. 4. (a) The memory complexity $\mathcal{C}_j^1$ and (b) the memory size $\mathcal{D}_j$ as a function of the time step j. The yellow (upper) and green (lower) dashed lines are results for pure and mixed system-environment initial states, respectively, while the yellow (upper) and green (lower) solid lines are the corresponding theoretical limits. The unitary evolutionary operator U is generated by Eq. (11) in the same way as Fig. 3, while the pure and mixed system-environment initial states are randomly generated and are entangled.

major extensions of the process tensor framework, which are summarized as follows: (1) We propose to work with the purified process tensor, which can be written as a matrix product state and is more informative compared to the process tensor since the site tensors of the PPT directly reveal the hidden OQE model (the 0th site tensor corresponds to the SE initial state and the rest correspond to the discrete unitary evolutionary operators). (2) We present an efficient purified process tensor tomography algorithm which scales linearly with the number of time step k. (3) We draw the deep connections between the quantum process and the classical stochastic process by showing the similar role of the hidden OQE for the quantum process and the ϵ-machine for the classical stochastic process; in particular we define the memory complexity and memory size for a quantum process, which are in parallel to the corresponding definitions for the ϵ-machine and which characterize the complexity of our reconstruction algorithm. Therefore, this work provides a systematic approach to fully characterize generic non-Markovian quantum dynamics based only on experimentally measurable quantities (multitime measurements), and it could be a useful technique to study non-Markovian noises on near-term quantum devices. A promising future research direction could be to study the non-Markovian memory effects induced by an infinite environment based on the purified process tensor.

The code for the numerical examples used in this work can be found at [44].

ACKNOWLEDGMENTS

C.G. would like to thank Chengran Yang for helpful discussions. C.G. acknowledges support from National Natural Science Foundation of China under Grant No. 11805279.

APPENDIX: DETAILED PROOF OF THEOREM 1

In case $\mathcal{U}$ is assumed time-independent, we have

$$\rho_j^E = \overleftarrow{T}^j\left(\rho_0^E\right); \tag{A1}$$

as a result ρ_j^E will converge to the left dominate eigenstate of T with the largest eigenvalue [22]. We assume that the dominate eigenstate of T is nondegenerate, which is similar to an ergodic requirement on $\mathcal{U}$ [39].

First, we will prove that any left eigenstate of T has an eigenvalue smaller or equal to 1. We will also use a single index σ_j to denote the tuple (i_{j-1}, o_j) for $j > 0$ for briefness. For any basis $|a\rangle\langle b|$ of the density matrix of the environment, we have

$$|\overleftarrow{T}(|a\rangle\langle b|)|^2 = \sum_{\sigma,\sigma',\alpha,\alpha'} \left(B^{\sigma}_{a,\alpha'}\right)^* B^{\sigma}_{b,\alpha} B^{\sigma'}_{a,\alpha'} \left(B^{\sigma'}_{b,\alpha}\right)^*. \tag{A2}$$

Now we define two matrices

$$X_a^{\sigma,\sigma'} = \sum_{\alpha'} B^{\sigma}_{a,\alpha'} \left(B^{\sigma'}_{a,\alpha'}\right)^*, \tag{A3}$$

$$Y_b^{\sigma,\sigma'} = \sum_{\alpha} B^{\sigma}_{b,\alpha} \left(B^{\sigma'}_{b,\alpha}\right)^*, \tag{A4}$$

which are semipositive and Hermitian matrices by definition. We can also see that $\mathrm{tr}(X) = \sum_{\alpha',\sigma} B^{\sigma}_{a,\alpha'} (B^{\sigma}_{a,\alpha'})^* = 1$ since B is right-canonical, and the same for Y. Then Eq. (A2) can be written as

$$\begin{aligned} |\overleftarrow{T}(|a\rangle\langle b|)|^2 &= \mathrm{tr}(X^\dagger Y) \leqslant \sqrt{\mathrm{tr}(X^\dagger X)}\sqrt{\mathrm{tr}(Y^\dagger Y)} \\ &= \sqrt{\mathrm{tr}(X^2)}\sqrt{\mathrm{tr}(Y^2)} \leqslant \sqrt{\mathrm{tr}^2(X)}\sqrt{\mathrm{tr}^2(Y)} \\ &= \mathrm{tr}(X)\mathrm{tr}(Y) = 1, \end{aligned} \tag{A5}$$

where the second step in the first line of Eq. (A5) follows from the Cauchy-Schwarz inequality, and the inequality in the second line is due to the semipositivity of X and Y. Equality holds only if $a = b$. Thus for any state $\rho = \sum_{a,b} \rho_{a,b}|a\rangle\langle b|$, we have

$$|\overleftarrow{E}(\rho)|^2 = \left|\sum_{a,b} \rho_{a,b} \overleftarrow{E}(|a\rangle\langle b|)\right|^2 \leqslant |\rho|^2 |\overleftarrow{E}(|a\rangle\langle b|)|^2 = |\rho|^2, \tag{A6}$$

and therefore any left eigenvector of T has an eigenvalue that is not greater than 1.

Second, we show that the maximally mixed state $\hat{I}^E/D$ is both a left and right eigenvector of T with eigenvalue 1. This immediately follows since B^σ is both left- and right-canonical (except for the first site, B^{o_0}, which does not matter for large time steps). Thus the first part of Theorem 1 is proved.

Now we proceed to prove the second part of Theorem 1 for mixed system-environment initial state. In this case we need to first purify the initial state with dD external basis $|x_s\rangle$ as

$$\left|\rho_0^{SE}\right\rangle = \sum_s \lambda_s |x_s\rangle|y_s\rangle. \tag{A7}$$

Accordingly the site matrix should be enlarged to

$$B^{\sigma'} = B^\sigma \otimes I^{SE}. \tag{A8}$$

The enlarged transfer matrix $T' = \sum_{\sigma'} (B^{\sigma'})^* \otimes B^{\sigma'}$ is certainly degenerate. We note that the traceless matrices span a linear subspace which is orthogonal to the maximally entangled state and that the transfer matrix maps only traceless matrices to traceless matrices due to trace preservation. Then since the largest eigenvalue is assumed to be nondegenerate, all the traceless matrices must have eigenvalues strictly less than 1. From Eq. (A7), the enlarged effective environment state $\rho_0^{E'}$, which includes the original environment plus the external basis $|x_s\rangle$, can be written as

$$\rho_0^{E'} = \sum_{s,s'} \lambda_s \lambda_{s'} |x_s\rangle\langle x_{s'}| \otimes \mathrm{tr}_S(|y_s\rangle\langle y_{s'}|). \tag{A9}$$

Then we have

$$\rho_j^{E'} = \overleftarrow{T'}^j\left(\rho_0^{E'}\right) = \sum_{s,s'} \lambda_s \lambda_{s'} |x_s\rangle\langle x_{s'}| \otimes \overleftarrow{T'}^j[\mathrm{tr}_S(|y_s\rangle\langle y_{s'}|)]. \tag{A10}$$

For $s \neq s'$, we have $\mathrm{tr}_E[\mathrm{tr}_S(|y_s\rangle\langle y_{s'}|)] = \langle y_{s'}|y_s\rangle = 0$, namely, $\mathrm{tr}_S(|y_s\rangle\langle y_{s'}|)$ is a traceless density matrix of the environment. Thus from the previous arguments the state $\mathrm{tr}_S(|y_s\rangle\langle y_{s'}|)$ lives in a subspace with eigenvalue strictly less than 1, and we have $\overleftarrow{T'}^\infty[\mathrm{tr}_S(|y_s\rangle\langle y_{s'}|)] = 0$. As a result, for $j \to \infty$, Eq. (A10) becomes

$$\rho_\infty^{E'} = \sum_s \lambda_s^2 |x_s\rangle\langle x_s| \otimes I^E/D. \tag{A11}$$

Thus the second part of Theorem 1 has been proved.

[1] I. de Vega and D. Alonso, Rev. Mod. Phys. **89**, 015001 (2017).
[2] E. Sudarshan, P. Mathews, and J. Rau, Phys. Rev. **121**, 920 (1961).
[3] T. F. Jordan and E. Sudarshan, J. Math. Phys. **2**, 772 (1961).
[4] A. J. Leggett, S. Chakravarty, A. T. Dorsey, M. P. Fisher, A. Garg, and W. Zwerger, Rev. Mod. Phys. **59**, 1 (1987).
[5] F. Arute, K. Arya, R. Babbush, D. Bacon, J. C. Bardin, R. Barends *et al.*, Nature (London) **574**, 505 (2019).
[6] Y. Wu, W.-S. Bao, S. Cao, F. Chen, M.-C. Chen, X. Chen *et al.*, Phys. Rev. Lett. **127**, 180501 (2021).
[7] Q. Zhu, S. Cao, F. Chen, M.-C. Chen, X. Chen *et al.*, Sci. Bull. **67**, 240 (2022).
[8] I. L. Chuang and M. A. Nielsen, J. Mod. Opt. **44**, 2455 (1997).
[9] G. M. D'Ariano and P. Lo Presti, Phys. Rev. Lett. **86**, 4195 (2001).
[10] Á. Rivas, S. F. Huelga, and M. B. Plenio, Phys. Rev. Lett. **105**, 050403 (2010).
[11] S. C. Hou, X. X. Yi, S. X. Yu, and C. H. Oh, Phys. Rev. A **83**, 062115 (2011).
[12] C. R. Shalizi, Causal architecture, complexity and self-organization in time series and cellular automata, Ph.D. dissertation, University of Wisconsin–Madison, 2001.
[13] S. Milz, F. A. Pollock, and K. Modi, Open Syst. Inf. Dyn. **24**, 1740016 (2017).
[14] F. Costa and S. Shrapnel, New J. Phys. **18**, 063032 (2016).
[15] F. A. Pollock, C. Rodríguez-Rosario, T. Frauenheim, M. Paternostro, and K. Modi, Phys. Rev. A **97**, 012127 (2018).
[16] C. R. Shalizi and J. P. Crutchfield, J. Stat. Phys. **104**, 817 (2001).
[17] G. A. L. White, F. A. Pollock, L. C. L. Hollenberg, K. Modi, and C. D. Hill, PRX Quantum **3**, 020344 (2022).
[18] G. A. White, C. D. Hill, F. A. Pollock, L. C. Hollenberg, and K. Modi, Nat. Commun. **11**, 6301 (2020).
[19] L. Xiang, Z. Zong, Z. Zhan, Y. Fei, C. Run, Y. Wu, W. Jin, C. Xiao, Z. Jia, P. Duan *et al.*, arXiv:2105.03333 (2021).
[20] K. Goswami, C. Giarmatzi, C. Monterola, S. Shrapnel, J. Romero, and F. Costa, Phys. Rev. A **104**, 022432 (2021).
[21] R. Orús, Ann. Phys. **349**, 117 (2014).
[22] U. Schollwöck, Ann. Phys. **326**, 96 (2011).
[23] F. Verstraete, J. J. Garcia-Ripoll, and J. I. Cirac, Phys. Rev. Lett. **93**, 207204 (2004).
[24] G. De las Cuevas, N. Schuch, D. Pérez-García, and J. I. Cirac, New J. Phys. **15**, 123021 (2013).
[25] J. Guth Jarkovský, A. Molnár, N. Schuch, and J. I. Cirac, PRX Quantum **1**, 010304 (2020).
[26] C. Guo, Phys. Rev. B **105**, 195152 (2022).
[27] C. Schön, E. Solano, F. Verstraete, J. I. Cirac, and M. M. Wolf, Phys. Rev. Lett. **95**, 110503 (2005).
[28] D. Gross, Y.-K. Liu, S. T. Flammia, S. Becker, and J. Eisert, Phys. Rev. Lett. **105**, 150401 (2010).
[29] M. Cramer, M. B. Plenio, S. T. Flammia, R. Somma, D. Gross, S. D. Bartlett, O. Landon-Cardinal, D. Poulin, and Y.-K. Liu, Nat. Commun. **1**, 149 (2010).
[30] T. Baumgratz, D. Gross, M. Cramer, and M. B. Plenio, Phys. Rev. Lett. **111**, 020401 (2013).
[31] B. Lanyon, C. Maier, M. Holzäpfel, T. Baumgratz, C. Hempel, P. Jurcevic, I. Dhand, A. Buyskikh, A. Daley, M. Cramer *et al.*, Nat. Phys. **13**, 1158 (2017).
[32] C. Guo, Z. Jie, W. Lu, and D. Poletti, Phys. Rev. E **98**, 042114 (2018).
[33] C. Guo, K. Modi, and D. Poletti, Phys. Rev. A **102**, 062414 (2020).
[34] R. Fletcher, *Practical Methods of Optimization* (John Wiley & Sons, New York, 2013).
[35] C. Guo and D. Poletti, Phys. Rev. E **103**, 013309 (2021).
[36] F. C. Binder, J. Thompson, and M. Gu, Phys. Rev. Lett. **120**, 240502 (2018).
[37] T. J. Elliott and M. Gu, npj Quantum Inf. **4**, 18 (2018).
[38] T. J. Elliott, C. Yang, F. C. Binder, A. J. P. Garner, J. Thompson, and M. Gu, Phys. Rev. Lett. **125**, 260501 (2020).
[39] C. Yang, F. C. Binder, V. Narasimhachar, and M. Gu, Phys. Rev. Lett. **121**, 260602 (2018).
[40] N. Barnett and J. P. Crutchfield, J. Stat. Phys. **161**, 404 (2015).
[41] T. J. Elliott, M. Gu, A. J. P. Garner, and J. Thompson, Phys. Rev. X **12**, 011007 (2022).
[42] A. J. Daley, H. Pichler, J. Schachenmayer, and P. Zoller, Phys. Rev. Lett. **109**, 020505 (2012).
[43] R. Islam, R. Ma, P. M. Preiss, M. Eric Tai, A. Lukin, M. Rispoli, and M. Greiner, Nature (London) **528**, 77 (2015).
[44] https://github.com/guochu/QuantumMemoryComplexity.